U-UV Coding for Bit-Interleaved Coded Modulation

Changyu Wu, Wenhao Chen, Li Chen, *Senior Member, IEEE*, and Huazi Zhang, *Senior Member, IEEE*

***Abstract*— U-UV codes were recently proposed as a competent short-to-medium length coding scheme. With well designed component codes, U-UV codes can outperform similar rate cyclic redundancy check (CRC)-polar codes with the successive cancellation (SC) and the SC list (SCL) decoding. In order to improve the coded transmission spectral efficiency, this paper proposes the bit-interleaved coded modulation (BICM) scheme with U-UV codes as the channel codes. A bit interleaver structure is proposed to facilitate the component code rate allocation based on the polarized subchannel capacities. Under the BICM paradigm, the component code rates can be allocated by first estimating the modulation subchannel capacities, then adjusting based on the finite length rates and the equal error probability rule. Theoretical performance bounds and their approximations on decoding error rates are further analyzed. It provides the theoretical benchmarks for our simulations and guides the optimized design of the coded modulation scheme. Finally, simulation results of the U-UV coded BICM scheme are provided to demonstrate its error-correction competency. It can outperform the relevant bit-interleaved polar coded modulation (BIPCM) scheme.**

***Index Terms*— Bit-interleaved coded modulation, spectral efficiency, U-UV codes.**

I. Introduction

FUTURE communication systems will realize ultra reliable and low-latency information transmission, for which competent short-to-medium length channel codes are important. So far, the good performing short-to-medium length codes include the Bose-Chaudhuri-Hocquenghem (BCH) codes [1], [2], the tail-biting convolutional codes [3], the cyclic redundancy check (CRC)-polar codes [1] [4], [5], [6], and the more recent polarization adjusted convolutional (PAC) codes [7]. The ordered statistics decoding (OSD) is able to achieve a near maximum likelihood (ML) decoding performance for BCH codes, but inherits a complexity that grows exponentially with its decoding order [8]. The CRC-polar codes can also achieve a near ML performance with the successive cancellation list (SCL) decoding [5], [6]. Although well designed CRC-polar codes [9], [10] can further enhance the performance, channel polarization remains incomplete in the short-to-medium length regime. There exists a significant portion of subchannels without a polarized capacity. They cannot be adequately utilized, resulting in a capacity loss. Note that polar codes have been proven to achieve capacity of the binary input symmetric discrete memoryless channel as codeword length is sufficiently large [4]. To overcome the incomplete polarization, PAC codes were recently proposed by introducing an outer convolutional transform. It helps reallocate the transmission of the unpolarized subchannels.

Another solution for the incomplete polarization can be realized through U-UV structural coding [11], [12]. It is a re-exploration of the classic Plotkin codes [13], in which the U codes and V codes are component codes of equal length. They are concatenated in a $(\mathrm{U}\,|\,\mathrm{U}+\mathrm{V})$ recursive manner. For succinctness, we use U-UV to refer this $(\mathrm{U}\,|\,\mathrm{U}+\mathrm{V})$ coding structure. This structural coding also results in polarized subchannel capacities. Each of the subchannels conveys a component codeword. Consequently, the component code rates can be designed accordingly. Compared with CRC-polar codes, it does not require complete polarization of the subchannel capacities. Moreover, Its decoding parallelism can be realized through the component code decoding, leading to a greater potential of achieving a low decoding latency than the CRC-polar codes. With BCH component codes, the U-UV code is also known as the generalized BCH-polar concatenated codes [14]. It has been shown that the U-UV codes can outperform the CRC-polar codes using either the successive cancellation (SC) decoding or the SCL decoding [11]. Hence, the U-UV codes appear to be another good performing short-to-medium length code. To realize the spectrally efficient coded transmission, U-UV codes' integration with high order modulation schemes should be studied, which is the primary motivation of this work.

Coded modulation integrates the design of a channel code and a high order modulation scheme, which can be realized through multilevel coding (MLC) [15], trellis coded modulation (TCM) [16] or bit-interleaved coded modulation (BICM) [17], [18]. Among them, BICM has been employed in several communication systems, including wireless LANs, WiMax and cellular networks. A BICM scheme bridges a channel code and a high order modulation scheme by the bit interleavers. Its parallel channel model decomposes the high order channel input into a set of bit channels. Independent binary encoding and decoding are realized in each bit channel so that the powerful family of binary codes can be integrated with a high order signal constellation. The bit interleavers diversify the transmission of the neighboring coded bits, combating

Manuscript received 21 November 2022; revised 3 April 2023 and 14 June 2023; accepted 15 June 2023. Date of publication 26 June 2023; date of current version 18 September 2023. This work is sponsored by the National Natural Science Foundation of China (NSFC) with project ID 62071498. The associate editor coordinating the review of this article and approving it for publication was A. E. Pusane. *(Corresponding author: Li Chen.)*

Changyu Wu is with the School of Electronics and Communication Engineering, Sun Yat-sen University, Guangzhou 510006, China (e-mail: wuchy28@mail2.sysu.edu.cn).

Wenhao Chen and Li Chen are with the School of Electronics and Information Technology, Sun Yat-sen University, Guangzhou 510006, China (e-mail: chenwh85@mail2.sysu.edu.cn; chenli55@mail.sysu.edu.cn).

Huazi Zhang is with the Hangzhou Research Center, Huawei Technologies Company Ltd., Hangzhou 310052, China (e-mail: zhanghuazi@huawei.com).

Color versions of one or more figures in this article are available at https://doi.org/10.1109/TCOMM.2023.3289579.

Digital Object Identifier 10.1109/TCOMM.2023.3289579

[1]They are modified polar codes with the outer concatenated CRC codes.

the channel fading effects. However, it should be pointed out that a BICM scheme is suboptimal due to the independence assumption of the decomposed bit channels. This loss can be compensated by the iterative decoding (ID) between the demodulator and the decoder, i.e., the BICM-ID [19].

The bit-interleaved polar coded modulation (BIPCM) [20], [21], [22] integrates polar codes and the BICM structure. It has also been adopted in the 5G wireless communication standard [23]. The channel partition theory was proposed to analyze the BIPCM schemes [20]. The integration of polar codes and different order modulations can also be realized by the concept of virtual channel [21], where the polarized subchannel reliability can be evaluated using the Bhattacharyya parameter. On the other hand, compound polar codes [22] was introduced to adapt to the modulation order by introducing an additional polarization matrix. It increases polarization and yields an improved decoding performance. A BIPCM scheme for 64-QAM was also proposed based on the multi-kernel polar codes [24]. The partially information coupled BIPCM was proposed in [25], which can also be seen as an effort to overcome the incomplete polarization of short-to-medium length polar codes. With the weight enumerating function, a BIPCM scheme and a non-binary interleaved polar coded modulation scheme were designed based on the polarization effect and the block error rate upper bound [26], [27]. A constellation shaping method and labeling strategy for BIPCM were proposed in [28] and [29], respectively. Besides BIPCM, there also exist work focusing on the design of multi-level polar coded modulation (MLPCM) [20], [30], [31], [32], [33], [34], [35], [36]. Recently, a hybrid polar coded modulation scheme that features both the BICM and the MLC was propsed to achieve a better tradeoff between the decoding latency and performance [37].

In order to realize spectrally efficient transmission for the U-UV coded systems, this paper proposes the U-UV coded BICM scheme. The main contributions of this work are as follows:

- Intrinsic structure of the bit interleaver is designed so that the diversified bit channel capacities of the modulation scheme can be rationally utilized, which also facilitates the rate allocation of the component codes.
- A comprehensive strategy is proposed for allocating the component code rates, so that the designed U-UV coded BICM scheme cannot only achieve a targeted information rate[2], but also yield a good decoding performance. Two rate allocation algorithms that estimate the polarized subchannel capacities are first introduced, which are based on the Bhattacharyya parameter and the Gaussian approximation (GA), respectively. Based on the estimated subchannel capacities, the finite length rate and the equal error probability rule are further applied to adjust the component code rates.
- Decoding performance bounds and their approximations of the U-UV coded BICM schemes are further analyzed, providing the theoretical performance benchmarks for our simulations. This analysis also helps optimize the interleaver design.
- Utilizing BCH codes as the component codes, extensive simulations on the proposed U-UV coded BICM schemes have been carried out. Our simulation results demonstrate the effectiveness of the proposed BICM scheme design. They also show that substantial performance gains can be achieved over the BIPCM schemes that employ CRC-polar codes.

[2]It is the number of information bits carried by each transmitted symbol.

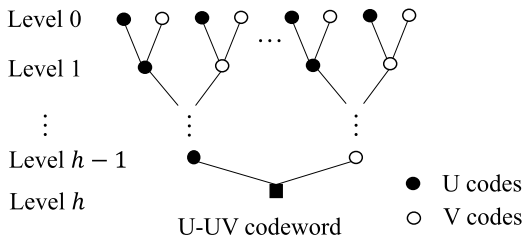

Fig. 1. Construction of an h levels U-UV code.

The rest of this paper is organized as follows. Section II proposes the U-UV coded BICM scheme. Section III presents two rate allocation algorithms and further adjustments to allocate the component code rates. Theoretical performance bounds and their approximations of the U-UV coded BICM schemes are studied in Section IV. Section V presents our simulation results and discussions. Finally, Section VI concludes the paper.

II. U-UV Coded BICM

This section introduces the U-UV coded BICM schemes, including the encoding of the U-UV codes and the following coded modulation. Finally, the demodulation and decoding will be introduced.

A. U-UV Codes

Consider the U code and V code are two binary block codes, denoted as $\mathbb{C}_{\mathrm{U}}$ and $\mathbb{C}_{\mathrm{V}}$, respectively. They have a length of n and a dimension of k_{U} and k_{V}, respectively. A single level U-UV code, denoted as $\mathbb{C}_{\text{U-UV}}$, is a block code of length $2n$ and dimension $k_{\mathrm{U}}+k_{\mathrm{V}}$. It is constructed with $\mathbb{C}_{\mathrm{U}}$ and $\mathbb{C}_{\mathrm{V}}$ in the U-UV manner as [13]

$$\mathbb{C}_{\text{U-UV}} = \{(\boldsymbol{c}_{\mathrm{U}} \mid \boldsymbol{c}_{\mathrm{U}} + \boldsymbol{c}_{\mathrm{V}}) : \boldsymbol{c}_{\mathrm{U}} \in \mathbb{C}_{\mathrm{U}}, \boldsymbol{c}_{\mathrm{V}} \in \mathbb{C}_{\mathrm{V}}\}, \quad (1)$$

where $\boldsymbol{c}_{\mathrm{U}}$ and $\boldsymbol{c}_{\mathrm{V}}$ are the codeword of $\mathbb{C}_{\mathrm{U}}$ and $\mathbb{C}_{\mathrm{V}}$, respectively. When more component codes are involved, this construction can be extended recursively, resulting in a multilevel construction. Fig. 1 illustrates the construction of an h levels U-UV code. At level 0, there are $\gamma = 2^h$ component codes of length n. They are coupled in the U-UV manner as in (1) to construct the U-UV codes of level 1. The U-UV codewords at level 1 can again be used as the U codes and V codes to construct to the U-UV codewords of level 2. This U-UV construction can be extended recursively, and finally an h levels construction will yield a U-UV codeword of length $N = \gamma n$. By specifying the component codes at level 0, the U-UV code can also be seen as a generalized concatenated code (GCC) with inner polar codes [14], [38], [39], [40], [41], [42].

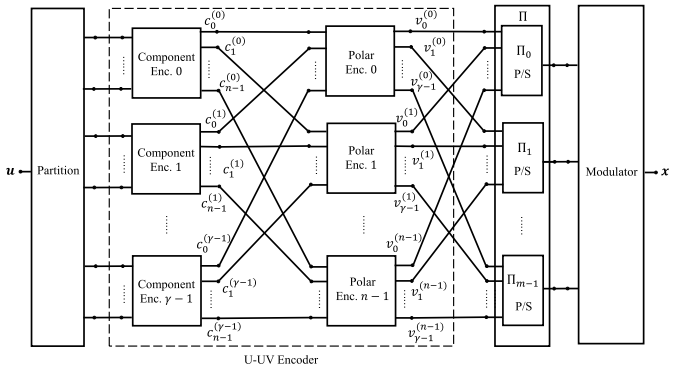

Fig. 2. Block diagram of the U-UV coded BICM scheme with $\gamma = m$.

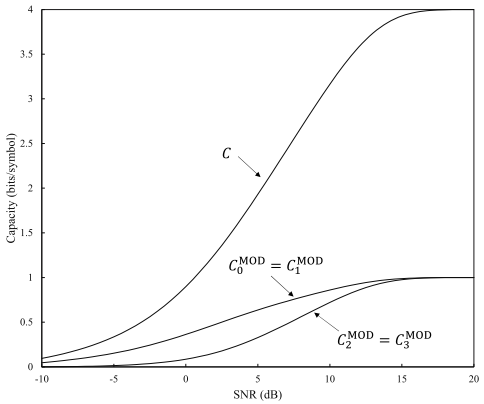

Fig. 3. Bit channel capacities of the Gray labeling 16-QAM.

E.g., if BCH codes are utilized as the component codes, the U-UV code can be seen as a generalized BCH-polar concatenated code.

This U-UV code construction exhibits channel polarization effect [4], resulting in γ *subchannels* with polarized capacities at level 0. We use W_i and C_i to denote the subchannels and their capacities, respectively, where $i = 0, 1, \ldots, \gamma - 1$. Each subchannel conveys a component codeword. Hence, the subchannels are also known as the vector channels of length n. Let $\mathbb{C}_i$ denote the component code (the U code or the V code) that is transmitted through subchannel W_i. It has a dimension of k_i and a rate of $r_i = k_i/n$. As a result, the U-UV code has a dimension of $K = \sum_{i=0}^{\gamma-1} k_i$ and a rate of $R = K/N$. The component code rates can be designed based on several rate allocation strategies. E.g., it has been proposed in [14] and [38] that the component code rates can be designed based on equalling their decoding error probabilities. The following Section III will introduce a more comprehensive rate allocation strategy for the U-UV coded BICM schemes, resulting in less rate loss.

B. The Proposed Coded Modulation

Block diagram of the proposed U-UV coded BICM scheme can also be represented in the GCC paradigm, as shown in Fig. 2. There are γ outer component codes and n inner polar codes. The outer codes and inner codes are of length n and γ, respectively. Since $\gamma = 2^h$, the inner polar codes have h polarization steps. Referring to the h levels U-UV code construction of Fig. 1, the outer component encoders generate component codewords at level 0, and the inner polar encoders correspond to the U-UV code construction from level 1 to level h as shown in Fig. 1. In particular, let

$$\boldsymbol{u} = (u_0, u_1, \ldots, u_{K-1}) \tag{2}$$

denote the binary message vector. Note that this work considers binary codes. In the U-UV encoding, $\boldsymbol{u}$ is partitioned into γ blocks of length $k_0, k_1, \ldots, k_{\gamma-1}$, respectively. Each of them will be encoded by an outer component code. Let $\boldsymbol{c}_{(i)} = (c_0^{(i)}, c_1^{(i)}, \ldots, c_{n-1}^{(i)})$ denote the ith component codeword, where $i = 0, 1, \ldots, \gamma - 1$. Input of the jth polar encoder is $(c_j^{(0)}, c_j^{(1)}, \ldots, c_j^{(\gamma-1)})$, i.e., the jth symbol of all component codewords, where $j = 0, 1, \cdots, n - 1$. Output of the jth polar encoder is $(v_0^{(j)}, v_1^{(j)}, \ldots, v_{\gamma-1}^{(j)})$. Note that the bit reversal operation [4] is contained within the polar encoders. The U-UV codeword $\boldsymbol{v}$ is obtained by cascading the output of all the inner polar encoders as

$$\begin{aligned}\boldsymbol{v} = (&v_0^{(0)}, v_0^{(1)}, \ldots, v_0^{(n-1)}, \quad v_1^{(0)}, v_1^{(1)}, \ldots, v_1^{(n-1)}, \\ &\times \ \ldots \ \ldots, v_{\gamma-1}^{(0)}, v_{\gamma-1}^{(1)}, \ldots, v_{\gamma-1}^{(n-1)}).\end{aligned} \tag{3}$$

Let us assume that the U-UV code is integrated with a modulation scheme of order m. With ideal interleaving, the system can be equivalently modelled as a set of m parallel binary input channels [18]. They are distinguished by the label indices of a signal constellation. Given a 2^m-ary modulation, let $\mathcal{X}$ denote the modulated symbol set and $\mathcal{X}_p^\mu$ further denote a subset of $\mathcal{X}$ with their pth labelling bit being μ, where $p = 0, 1, \ldots, m - 1$ and $\mu \in \{0, 1\}$. Given a modulation symbol set $\mathcal{X}$ and a received symbol y, the pth bit channel can be defined by its transition probability.

$$P_p(y|\mu) = \frac{1}{2^{m-1}} \sum_{x \in \mathcal{X}_p^\mu} P_{\mathcal{Y}|\mathcal{X}}(y|x), \tag{4}$$

where $P_{\mathcal{Y}|\mathcal{X}}(\cdot|\cdot)$ is the transition probability of the underlying channel with input $\mathcal{X}$ and output $\mathcal{Y}$. Capacity of the pth bit channel can be further determined by [18]

$$C_p^{\mathrm{MOD}} = 1 - \mathbb{E}\left[\log_2 \frac{\sum\limits_{x \in \mathcal{X}} P_{\mathcal{Y}|\mathcal{X}}(y|x)}{\sum\limits_{x \in \mathcal{X}_p^\mu} P_{\mathcal{Y}|\mathcal{X}}(y|x)}\right]. \tag{5}$$

In particular, when it is the additive white Gaussian noise (AWGN) channel, the transition probability is

$$P_{\mathcal{Y}|\mathcal{X}}(y|x) = \frac{1}{\sqrt{2\pi}\sigma} e^{-\frac{||y-x||^2}{2\sigma^2}}, \tag{6}$$

where σ^2 is the noise variance. Fig. 3 shows the bit channel capacities of the Gray labeling 16-QAM against the AWGN channel signal-to-noise ratio (SNR). Capacities of the four bit channels which are denoted as C_0^{MOD}, C_1^{MOD}, C_2^{MOD} and C_3^{MOD}, respectively, have two possible values. Capacity C of the 16-QAM is the sum of its decomposed bit channel capacities. In the following, we call these bit channels the *modulation channels*.

With the above mentioned setup, the U-UV coded BICM process can be described as follows. The message $\boldsymbol{u}$ is encoded by the U-UV encoder, yielding a codeword of (3). The codeword symbols are fed into an interleaver Π which

performs bit wise permutation. As Fig. 2 shows, the modulator further arranges every m interleaved coded bits in groups and maps them into a sequence of modulated symbols $\boldsymbol{x} = (x_0, x_1, \ldots, x_{N/m-1})$, where it is assumed that $m|N$. Each modulated symbol x_t has a bit label of $(x_t^{(0)} x_t^{(1)} \cdots x_t^{(m-1)})$, where $t = 0, 1, \ldots, N/m-1$. $x_t^{(p)}$ is a constituent bit of x_t, which will be transmitted through the pth modulation channel. Let $v_\omega^{(j)}$ denote the jth polar encoder output, where $\omega = 0, 1, \ldots, \gamma - 1$ and $j = 0, 1, \ldots, n-1$. Therefore, the interleaver is a bijective mapper $\Pi : (j, \omega) \mapsto (p, t)$, which designates the modulation channel and the modulated symbol sequence index for each U-UV coded bit. That says given $\Pi(\cdot)$ as the interleaving function, we have $x_t^{(p)} = \Pi(v_\omega^{(j)})$.

The coded bits are conveyed through different equivalent modulation channels, which have different capacities. There exists intrinsic channel polarization effect within the U-UV coding structure. It is assumed that all inner polar encoders can provide the identical bundles of the polarized subchannels, so that the strategies for assigning the component code rates can be derived. Therefore, for the output of each polar encoder, the mapping from codeword symbols to modulation channels will be the same. Let $\mathcal{M}(\omega)$ denote the index of the modulation channel which conveys the coded bit $v_\omega^{(j)}$ for all j. We call the mapping $\mathcal{M} : \omega \mapsto p$ the *interleaving pattern*. This pattern should be applied to the output of all inner polar encoders. Hence, the coded bits from the same position of different polar encoders should be sent to the same modulation channel. As shown in Fig. 2, the interleaver Π consists of m sub-interleavers $\Pi_0, \Pi_1, \ldots, \Pi_{m-1}$ of the same length. A sub-interleaver collects and permutes only the coded bits for its corresponding modulation channel.

For simplicity, it is assumed that the number of modulation channels is not greater than that of component codes, i.e., $m \leq \gamma$. As mentioned above, it is required that the interleaving pattern should be the same for the output of each inner polar code. Therefore, if $\gamma \nmid m$, $\gamma \bmod m$ virtual modulation channels can be added [21]. The bits sent to the virtual modulation channels are punctured but resumed at the receiver for the demodulation and decoding.

C. Demodulation and Decoding

With a received symbol sequence $\boldsymbol{y} = (y_0, y_1, \ldots, y_{N/m-1}) \in \mathcal{Y}^{N/m}$, the *a posteriori* probabilities (APPs) of the interleaved coded bits can be determined by

$$P(x_t^{(p)} = \mu) = \sum_{x \in \mathcal{X}_p^\mu} P(x) P_{\mathcal{Y}|\mathcal{X}}(y_t|x). \tag{7}$$

It is assumed that the constellation symbols are uniformly distributed, i.e., $P(x) = |\mathcal{X}|^{-1}, \forall x \in \mathcal{X}$. The log-likelihood ratio (LLR) of bit $x_t^{(p)}$ can be further determined by

$$L(x_t^{(p)}) = \ln \frac{P(x_t^{(p)} = 0)}{P(x_t^{(p)} = 1)}. \tag{8}$$

With the interleaving function, LLR values of the U-UV coded bits can be retrieved as $L(v_\omega^{(j)}) = L(\Pi(v_\omega^{(j)}))$. Since $x_t^{(p)} = \Pi(v_\omega^{(j)})$, we have $L(v_\omega^{(j)}) = L(x_t^{(p)})$. So that, the U-UV codeword can be decoded by the SC or SCL decoding mechanism [11], [43].

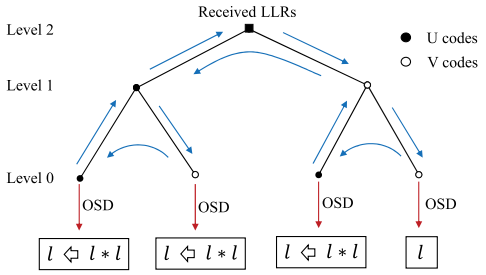

Fig. 4. SCL decoding process of a 2 levels U-UV code.

The SC decoding is the basic decoding mechanism for the U-UV codes. To improve the decoding performance, the SCL decoding further preserves multiple component codeword estimations, resulting in a list decoding approach which can be parameterized by its list size l. It yields an improved error-correction capability over the SC decoding. Fig. 4 shows the SCL decoding process of a 2 levels U-UV code, which can be extended to the case of multilevel construction. In the decoding, the LLR values that correspond to the component codeword symbols at level 0 are computed via the SC computational mechanism [4] based on the received LLRs at level h that are defined as in (8). Once the LLR values corresponding to a component codeword at level 0 are determined, the component code will be decoded by a particular decoding algorithm. E.g., in this work, the OSD is employed to decode the BCH component codes. The component codes are decoded successively. With a component codeword estimation, the correlation distance between the received information and the estimation will be calculated. It will be accumulated as more component codes are decoded, yielding the accumulated correlation distance [11], [43]. This becomes the likelihood metric of each decoding path. The l most likely U-UV codeword estimations correspond to the paths that yield the l smallest accumulated correlation distances. When $l = 1$, the SCL decoding degenerates into the SC decoding. In the OSD of an (n, k) binary linear block code with the minimum Hamming distance $d_{\min}$ and rate $k/n \geq 1/2$, its decoding order of

$$\tau = \min\left\{ \left\lfloor \frac{d_{\min}}{4} \right\rfloor, k \right\} \tag{9}$$

would be sufficient to yield an ML decoding performance for the code [8].

III. Rate Allocation

With the above mentioned U-UV coded BICM scheme, rate of each component code can be designed through combining several existing techniques. This will result in a U-UV coded BICM scheme that achieves a targeted information rate and also yields a good decoding performance. The subchannel capacities are first estimated for which two algorithms are introduced. They are based on the Bhattacharyya parameter [45] and the Gaussian approximation [38], respectively. Since the component codes are of short-to-medium length, they are not capacity approaching codes. Their rates are further adjusted by calculating the finite length rate over

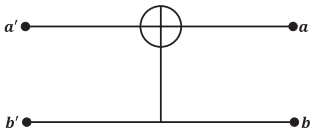

Fig. 5. Arßkan's basic polar kernel.

the subchannels. Finally, the equal error probability rule is applied to further adjust the component code rates, ensuring the decoding performance of the designed U-UV coded BICM.

A. Bhattacharyya Parameter

Let W denote a binary-input discrete memoryless channel with transition probability $P_{\mathrm{W}}(\cdot|\cdot)$. The Bhattacharyya parameter of W is defined as [45]

$$Z(\mathrm{W}) = \sum_{y\in\mathcal{Y}} \sqrt{P_{\mathrm{W}}(y|0)P_{\mathrm{W}}(y|1)}. \tag{10}$$

It can be utilized to determine the capacity of an arbitrary binary input discrete memoryless channel. If W is a binary erasure channel (BEC), its capacity is $C(\mathrm{W}) = 1 - Z(\mathrm{W})$. For a polar code, Bhattacharyya parameters of the polarized subchannels can be calculated recursively with the channel observations. For this, let us demonstrate Arßkan's basic polar kernel as shown in Fig. 5, whose nodes are indexed by a, a', b and b', respectively. With the knowledge of $Z(\mathrm{W}_a)$ and $Z(\mathrm{W}_b)$, under the BEC, the Bhattacharyya parameters of $\mathrm{W}_{a'}$ and $\mathrm{W}_{b'}$ can be computed as [4]

$$Z(\mathrm{W}_{a'}) = Z(\mathrm{W}_a) + Z(\mathrm{W}_b) - Z(\mathrm{W}_a)Z(\mathrm{W}_b) \tag{11}$$

and

$$Z(\mathrm{W}_{b'}) = Z(\mathrm{W}_a)Z(\mathrm{W}_b), \tag{12}$$

respectively. For the U-UV coded BICM scheme, the coded bits undergo different equivalent modulation channels. The initial condition for the recursive calculation is as follows. For each inner polar codeword position indexed by ω, its coded bits are sent to the $\mathcal{M}(\omega)$th modulation channel, and $Z(\mathrm{W}_\omega) = 1 - C^{\mathrm{MOD}}_{\mathcal{M}(\omega)}$. After the recursive calculation over the polar trellis[3], can be estimated by $C_i = 1 - Z(\mathrm{W}_i)$.

B. Gaussian Approximation

Gaussian approximation [38] is an alternative method for estimating the subchannel capacities with the underlying AWGN channel. Under this paradigm, the LLR values that are processed during the SC or the SCL decoding are assumed to be Gaussian distributed random variables. With the noise variance σ^2, the LLR values have a mean of $\mathbb{E}[L] = 2/\sigma^2$ and a variance of $\mathrm{var}[L] = 4/\sigma^2$, denoted as $L \sim \mathcal{N}(2/\sigma^2, 4/\sigma^2)$. Reliability of the polarized subchannels can be further derived. Referring to Arßkan's basic polar kernel shown in Fig. 5, let L_a, L_b, $L_{a'}$ and $L_{b'}$ denote the LLRs of nodes a, b, a' and b', respectively. Their means can be determined by

$$\mathbb{E}\left[L_{a'}\right] = \phi^{-1}\left(1 - \left(1 - \phi(\mathbb{E}\left[L_a\right])\right)\left(1 - \phi(\mathbb{E}\left[L_b\right])\right)\right), \tag{13}$$

$$\mathbb{E}\left[L_{b'}\right] = \mathbb{E}\left[L_a\right] + \mathbb{E}\left[L_b\right], \tag{14}$$

[3]Note that an h levels U-UV code can be represented by a polar trellis with h polarization steps.

where

$$\phi(z) = \begin{cases} 1 - \dfrac{1}{\sqrt{4\pi z}} \displaystyle\int_{-\infty}^{\infty} \tanh\left(\frac{\mu}{2}\right) e^{-\frac{(\mu - z)^2}{4z}} \mathrm{d}\mu, & z > 0 \\ 1, & z = 0 \end{cases}. \tag{15}$$

In the proposed U-UV coded BICM scheme, the modulation channels are assumed to be AWGN channels. With a design SNR ρ_d, the equivalent SNRs of the modulation channels can be determined based on (5). In particular, for a binary input AWGN (BIAWGN) channel, its capacity is a function of the SNR ρ as

$$C_{\mathrm{BIAWGN}}(\rho) = \frac{1}{2} \sum_{x\in\{0,1\}} \int_{-\infty}^{\infty} P(y|x) \log_2 \frac{P(y|x)}{\frac{1}{2} \sum\limits_{x'\in\{0,1\}} P(y|x')} \mathrm{d}y, \tag{16}$$

where the channel transition probability functions $P(\cdot|\cdot)$ are determined by ρ. With capacities of the modulation channels $C^{\mathrm{MOD}}_{\mathcal{M}(\omega)}$ derived from (5), the equivalent SNR values can be obtained by

$$\rho_\omega = C^{-1}_{\mathrm{BIAWGN}}(C^{\mathrm{MOD}}_{\mathcal{M}(\omega)}), \tag{17}$$

where C^{-1}_{BIAWGN} is the inverse function of the capacity function (16). Note that $C^{-1}_{\mathrm{BIAWGN}}(\cdot)$ is a monotonic function, it can be realized numerically. Since

$$\sigma^2_\omega = \frac{1}{2R} 10^{-\frac{\rho_\omega}{10}}, \tag{18}$$

where R is the code rate, the mean of the LLR values of each modulation channel can be determined by

$$\mathbb{E}\left[L_\omega\right] = \frac{2}{\sigma^2_\omega} = 4R \cdot 10^{\frac{\rho_\omega}{10}}. \tag{19}$$

For a full polar trellis, mean values of the LLRs $\mathbb{E}\left[L_i\right]$ at the information side can be calculated based on (13) and (14) recursively. Subsequently, the equivalent SNRs ρ_i of the polarization subchannels can be also derived from (19), i.e. $\rho_i = 10\log_{10}(\frac{\mathbb{E}[L_i]}{4R})$. Finally, the subchannel capacities can be determined based on (16) as

$$C_i = C_{\mathrm{BIAWGN}}(\rho_i). \tag{20}$$

Algorithm 1 summarizes this GA based capacity estimation method. Note that the Bhattacharyya parameter based capacity estimation algorithm is similar, with the only differences in the parameters and update formulas for the recursive calculation. In particular, lines 6 and 7 of **Algorithm 1** are replaced by $F[\omega] = 1 - C^{\mathrm{MOD}}_{\mathcal{M}(\omega)}$, lines 16 and 17 are updated by eq. (11) and eq. (12), respectively, and lines 23 and 24 are replaced by $C_i = 1 - F[\omega]$.

Note that the above subchannel capacity estimation provides references for component code rate allocation. It can be realized that the Bhattacharyya parameter based estimation is simpler, since it does not rely on the inverse functions that are otherwise needed by the GA method. However, estimating the equivalent SNRs of the modulation subchannels is beneficial in

Algorithm 1 GA Based Subchannel Capacities Estimation

Require: Design SNR ρ_d (in dB), U-UV coding level h;
Ensure: Subchannel capacities $\{C_0, C_1, \ldots, C_{\gamma-1}\}$;
for $p = 0, 1, \ldots, m-1$ **do**
  Compute C_p^{MOD} as in (5);
end for
Initialize an array F of length γ;
for $\omega = 0, 1, \ldots, \gamma-1$ **do**
  $\rho_\omega = C_{\text{BIAWGN}}^{-1}(C_{\mathcal{M}(\omega)}^{\text{MOD}})$;
  $F[\omega] = 4R \cdot 10^{\frac{\rho_\omega}{10}}$;
end for
for $i = 1, 2, \ldots, h$ **do**
  for $j = 0, 1, \ldots, 2^{h-i}-1$ **do**
    for $k = 1, 2, \ldots, 2^{i-1}$ **do**
      $\alpha \Leftarrow j \cdot 2^i + k$;
      $\beta \Leftarrow \alpha + 2^{i-1}$;
      $F_\alpha \Leftarrow F[\alpha]$;
      $F_\beta \Leftarrow F[\beta]$;
      $F[\alpha] \Leftarrow \phi^{-1}\left(1 - (1-\phi(F_\alpha))\,(1-\phi(F_\beta))\right)$;
      $F[\beta] \Leftarrow F_\alpha + F_\beta$;
    end for
  end for
end for
Perform bit reversal operation on F;
for $i = 0, 1, \ldots, \gamma-1$ **do**
  $\rho_i = 10 \cdot \log_{10}(\frac{F[i]}{4R})$;
  $C_i = C_{\text{BIAWGN}}(\rho_i)$;
end for

a more sophisticated design. E.g., the following subsection will show that the finite length rate calculation of the subchannels would require the equivalent SNRs. Moreover, Section IV will show that the theoretical performance analysis of the U-UV coded BICM scheme also requires them. Please note that both the above mentioned Bhattacharyya parameter based and the GA based subchannel capacity estimations would suffer an accuracy loss, which is incurred by the assumption of the channel models and perfect interleaving. Further considering the component codes are of short-to-medium length, they cannot achieve the subchannel capacities. In order to provide a more accurate rate allocation for the component codes and ensure the BICM scheme's error-correction performance, the finite length rate and the equal error probability rule should be further applied, which are introduced below.

C. Finite Length Rate

In the finite codeword length regime, the maximum transmission rate through a channel retreats from its channel capacity. This capacity loss is incurred by the channel dispersion [46]. Let $Q(\cdot)$ denote the complementary Gaussian cumulative distribution function as

$$Q(z) = \int_{-\infty}^{z} \frac{1}{\sqrt{2\pi}} e^{\frac{-\mu^2}{2}} \mathrm{d}\mu, \tag{21}$$

and $Q^{-1}(\cdot)$ denote its inverse. For the proposed BICM scheme, with the estimated equivalent SNR ρ_i, the maximum transmission rate of each component code can be further approximated by the normal approximation (NA) as

$$r_i^* \approx C(\mathrm{W}_i) - \left(\sqrt{\frac{D(\mathrm{W}_i)}{n}} Q^{-1}(P_{\mathrm{e}}) - \frac{\log_2 n}{2n}\right), \tag{22}$$

where P_{e} is the decoding error probability and

$$D(\mathrm{W}_i) \triangleq \sum_{x\in\mathcal{X}}\sum_{y\in\mathcal{Y}} \frac{1}{2} P_{\mathrm{W}_i}(y|x)\left(\log_2 \frac{P_{\mathrm{W}_i}(y|x)}{\frac{1}{2}\sum_{x'\in\mathcal{X}} P_{\mathrm{W}_i}(y|x')}\right)^2 - C(\mathrm{W}_i)^2 \tag{23}$$

is the dispersion of subchannel W_i. For the AWGN subchannel with noise variance σ_i^2, its dispersion can be reformulated as [46]

$$D(\mathrm{W}_i) = \frac{1}{\sqrt{2\pi}} \int e^{-\frac{\mu^2}{2}} \left(1 - \log_2\left(1 + e^{-\frac{2}{\sigma_i^2} + \frac{2\mu}{\sigma_i}}\right) - C(\mathrm{W}_i)\right)^2 \mathrm{d}\mu. \tag{24}$$

Hence, the rate of component code $\mathbb{C}_i$ should satisfy $r_i \le r_i^*$. Note that in case of capacity estimation based merely on the above mentioned Bhattacharyya parameter or GA, we have $r_i^* = C_i$.

Fig. 6 shows the component code rate allocation result of the 2 levels U-UV coded BICM scheme under the Gray labelling 16-QAM. The length of each component codeword is $n = 63$. Hence, the U-UV code is of length $N = 252$. The interleaving pattern is $\mathcal{M} : \{0,1,2,3\} \mapsto \{0,2,1,3\}$. With the maximum rate of each component code r_i^*, the maximum rate of the U-UV code is $R^* = \frac{1}{\gamma}\sum_{i=0}^{\gamma-1} r_i^*$. Fig. 6 shows both the Bhattacharyya parameter and the GA rate allocation results before and after considering the finite length rate. It can be seen that the finite length rates retreat from the Bhattacharyya parameter and the GA based estimations, providing a more practical rate allocation for the component codes.

D. Equal Error Probability Rule

Despite the U-UV code rates can be determined based on the estimated subchannel capacities and further adjusted by the finite length rates, the code's performance needs to be further optimized through equalling the component codes' decoding error probability. E.g., the equal error probability rule was utilized to derive a rate allocation algorithn for the component codes [14], [38]. However, it was designed for a specific channel SNR, which cannot guarantee the codes's performance for a wider range of channel conditions. In this work, instead of fomulating the design in an algorithmic fashion, we apply the equal error probability rule by aligning the component codes' decoding performances, leading to a U-UV code that can yield a good decoding performance for a wider range of channel SNR.

Let us again assume that each component code is transmitted through an equivalent AWGN channel with an approximated SNR ρ_i generated by one of the proposed subchannel capacity estimation algorithms. Once a component code has been determined by the above mentioned subchannel

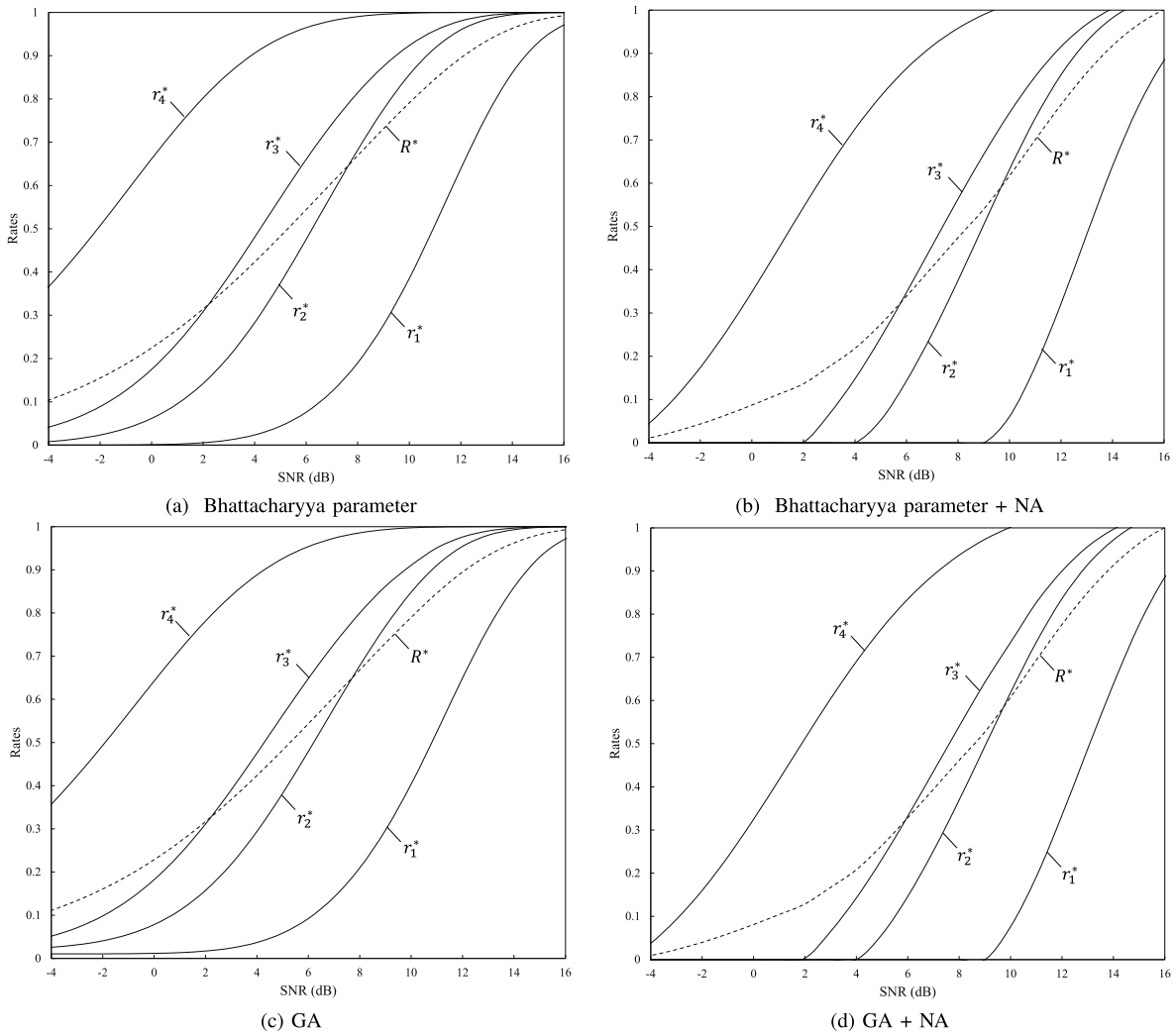

(a) Bhattacharyya parameter

(b) Bhattacharyya parameter + NA

(c) GA

(d) GA + NA

Fig. 6. Component code rate allocation of the 2 levels U-UV coded BICM with the Gray labelling 16-QAM.

capacity estimation and the finite length rate calculation, its weight spectrum can be further determined. Note that the weight spectrum for some algebraic codes can be determined by knowing its codeword length and dimension. E.g., both BCH codes and Reed-Solomon codes are equipped with this convenience. The ML decoding performance bounds, such as the tangential bound [49] can be further utilized to estimate their performance. Alternatively, the component codes' decoding performance can also be evaluated through simulations. If component codes' decoding error probabilities do not align, rate adjustment would be needed. Rates of the worse performing component codes should be slightly tuned down, while the opposite adjustment should be applied to the better performing component codes. This rate adjustment would enable the decoding error probabilities of all component codes better align, so that the decoding performance of the U-UV coded BICM scheme can be optimized. In this work, with a targeted information rate, we can estimate the subchannel capacities as in Section III-A and III-B. Afterwards, we can further design the component code rates based on both the above mentioned finite length rate and the equal error probability rules. We will demonstrate the effectiveness of this rate allocation strategy in Section V.

IV. Performance Analysis

This section analyzes the theoretical decoding performance bounds and their approximations for the U-UV coded BICM schemes. It provides theoretical benchmarks for our simulation results that will be presented in Section V. It also sheds light on the design of component codes and the bit interleaver. We will first analyze the approximated theoretical performance bounds for general U-UV coded BICM schemes, which can be applied to cases with any component codes. This analysis will then be specified with knowledge of component codes.

A. General U-UV Coded BICM

The approximated upper and lower bounds on the SC decoding frame error rate (FER) of polar concatenated codes over the AWGN channel has been characterized in [47]. They can be extended to analyze the U-UV coded BICM schemes. For a U-UV coding scheme, let S_i denote the successful decoding event of component code $\mathbb{C}_i$. Since the erroneous decoding (including the decoding errors and failures) of anyone of the component codes will lead to the erroneous decoding of the U-UV code, we let T_i denote the event that erroneous decoding first occurs in component code $\mathbb{C}_i$.

Its decoding error probability $P(T_i)$ can be determined by $P(T_i) = 1 - P(S_i|S_0, S_1, \ldots, S_{i-1})$. Based on Section III-C, it can be known that with the knowledge of code parameters and the channel condition, $P(T_i)$ can be approximated using the NA bound. Therefore, with γ component decoding events in decoding a U-UV code, the SC decoding error probability can be approximated by

$$P_{\mathrm{e}} = \sum_{i=0}^{\gamma-1} P(T_i) \approx \sum_{i=0}^{\gamma-1} Q\left(\frac{n(C_i - r_i) + \frac{1}{2}\log_2 n}{\sqrt{nD(\mathrm{W}_i)}}\right) \tag{25}$$

$$\leq \gamma \max_i Q\left(\frac{n(C_i - r_i) + \frac{1}{2}\log_2 n}{\sqrt{nD(\mathrm{W}_i)}}\right). \tag{26}$$

Note that (25) is derived by approximating $P(T_i)$ based on the NA bound of (22), which would be a good approximation when using powerful algebraic component codes such as BCH codes. Hence, eq. (26) is the approximated decoding FER upper bound. The subchannel capacities C_i can be estimated by the algorithms presented in Section III, while the calculation of the channel dispersion $D(\mathrm{W}_i)$ requires the assumption of a BIAWGN subchannel with its equivalent SNR value ρ_i. Further considering a rate R U-UV code which is designed by the component code rate allocation strategy of Section III, the approximated decoding FER upper bound can be further written as

$$P_{\mathrm{e}} \leq \gamma \min_{\substack{\{r_0, r_1, \ldots, r_{\gamma-1}\} \\ r_i \in [0, C_i] \\ \sum r_i = R}} \left\{ \max_i Q\left(\frac{n(C_i - r_i) + \frac{1}{2}\log_2 n}{\sqrt{nD(\mathrm{W}_i)}}\right)\right\}. \tag{27}$$

This constrained optimization problem can be solved efficiently by dynamic programming [47].

The above analysis leads to two approximated SC decoding FER upper bounds for the U-UV coded BICM schemes as eqs. (26) and (27). The approximated SC decoding FER lower bounds are provided as follows. With the SC decoding feature, the decoding error probability can be also determined by

$$\begin{aligned} P_{\mathrm{e}} &= 1 - P(S_0, S_1, \ldots, S_{\gamma-1}) \\ &= 1 - P(S_0)P(S_1|S_0)\cdots P(S_{\gamma-1}|S_0, S_1, \ldots, S_{\gamma-2}) \\ &= 1 - \prod_{i=0}^{\gamma-1}(1 - P(T_i)). \end{aligned} \tag{28}$$

In [48], an approximated decoding FER lower bound of the optimal codes over the (not necessarily binary input) AWGN channel is given. For a code of length n and rate r, its ML decoding error probability is

$$P_{\mathrm{e,AWGN}}(\rho, r, n) \approx \frac{1}{\sqrt{n\pi}} \frac{1}{\sqrt{1 + G^2}\sin\theta} \frac{\left[G\sin\theta e^{-\frac{1}{2\rho^2} + \frac{G\cos\theta}{2\rho}}\right]^n}{G\sin^2\theta/\rho - \cos\theta}, \tag{29}$$

where $G = 0.5\left(\cos\theta/\rho + \sqrt{\cos^2\theta/\rho^2 + 4}\right)$ and θ is the root of

$$\frac{\sqrt{2\pi n}\sin\theta\cos\theta}{\sin^n\theta} = 2^{nr}.$$

Therefore, based on eq. (28), the approximated lower bound for the U-UV coded BICM scheme can be written as

$$P_{\mathrm{e}} \geq 1 - \prod_{i=0}^{\gamma-1}\left[1 - P_{\mathrm{e,AWGN}}(\rho_i, r_i, n)\right] \tag{30}$$

The above lower bound is supported by assuming the ML decoding of all component codes. Similarly, considering all possible component code rate combinations, the decoding FER can be approximately lower bounded by

$$P_{\mathrm{e}} \geq \min_{\substack{\{r_0, r_1, \ldots, r_{\gamma-1}\} \\ r_i \in [0, C_i] \\ \sum r_i = R}} \left\{1 - \prod_{i=0}^{\gamma-1}\left[1 - P_{\mathrm{e,AWGN}}(\rho_i, r_i, n)\right]\right\}. \tag{31}$$

Finally, it should be pointed out that the approximated bounds of (27) and (31) provide the optimized performance benchmarks for the U-UV coded BICM schemes at any specified operating SNR.

B. U-UV Coded BICM With Specified Component Codes

By specifying the component codes, the decoding FER performance bounds and their approximations for a specific U-UV code can be further obtained. This often requires the knowledge of the component codes' weight spectra.

The tangential bound [49] is a tight ML decoding performance upper bound for any binary linear block code, which requires knowledge of the code's weight spectrum. For a linear block component code $\mathbb{C}_i$ with length n and minimum Hamming distance $d_{\min}$, let A_w denote the number of weight w codewords. Hence, $\{A_w | w = 0, d_{\min}, d_{\min} + 1, \ldots, n\}$ is the weight spectrum of the code. When transmitting over the AWGN channel, the decoding FER performance of $\mathbb{C}_i$ is upper bounded by [49]

$$\mathcal{T}(\mathbb{C}_i) = \sum_{w=0}^{n} A_w Q\left(-\frac{\sqrt{w}}{\sigma}\right) Q\left(-\frac{w - \theta}{\sigma\sqrt{n - w}}\right) + Q\left(-\frac{\theta}{\sigma}\right), \tag{32}$$

where θ is the root of

$$\sum_w A_w Q\left(\frac{\sqrt{\frac{w}{n-w}}(\sqrt{n} - \theta)}{\sigma}\right) = 1.$$

Based on the truncated union bound [45], the ML decoding FER performance of $\mathbb{C}_i$ for high SNR regime can be heuristically approximated by

$$\mathcal{U}(\mathbb{C}_i) = \frac{1}{2} A_{d_{\min}} \mathrm{erfc}\left(\sqrt{\frac{d_{\min} R E_{\mathrm{b}}}{2\sigma^2}}\right), \tag{33}$$

where E_{b} is the average energy per information bit and $\mathrm{erfc}(\cdot)$ is the complementary error function. Equipped with eqs. (32) and (33), the decoding FER upper bound of a specific U-UV code can be determined based on the tangential bounds of its component codes as

$$P_{\mathrm{e}} \leq \sum_{i=0}^{\gamma-1} \mathcal{T}(\mathbb{C}_i). \tag{34}$$

Meanwhile, its decoding FER at high SNR can be approximately lower bounded by

$$P_{\mathrm{e}} \geq \max_{i} \mathcal{U}(\mathbb{C}_i). \tag{35}$$

In this work, BCH component codes are utilized to substantiate the U-UV coded BICM scheme. Weight spectra of most short-to-medium length BCH codes are available in [50]. We will demonstrate the tightness of the above mentioned theoretical decoding performance benchmarks in the following Section V.

In the proposed U-UV coded BICM scheme, the interleaver design realizes the assignment of the coded bits to the modulation channels. When there are m modulation channels and γ component codes, there will be at most

$$\begin{aligned} |\mathcal{M}| &= \prod_{i=0}^{m-1} \binom{\tilde{\gamma} - i(\tilde{\gamma}/m)}{\tilde{\gamma}/m} \\ &= \tilde{\gamma}! \cdot [(\tilde{\gamma}/m)!]^{-m} \end{aligned} \tag{36}$$

interleaving patterns, where $\tilde{\gamma} = \gamma - (\gamma \mod m)$. Different interleaving patterns may yield the same subchannel capacity polarization. E.g., when $\tilde{\gamma} = m$ and m is even, there are at most $2^{-m/2} \prod_{i=0}^{m/2-1}(m-i)$ polarizations. The above derived performance bounds can also be utilized to identify interleaving pattern that yields a good performing BICM scheme. E.g., for a fixed rate U-UV code with specified component codes, the upper bound of (34) can be utilized to estimate the performance of different interleaving patterns. For a scheme that has the adequate amount of interleaving patterns, we can traverse them to find the optimal design. Also note that for different code rates, the optimal interleaving pattern for the U-UV coded BICM scheme may differ. With a modulation scheme, a joint design of interleaving pattern and component code rates would be desired. However, this becomes an exhaustive process with a formidable complexity. In this work, we first select an interleaving pattern. The component code rates then can be allocated by the method of Section III. Consequently, the decoding FER upper bound of (34) will be calculated. Repeating this performance evaluation over several candidate interleaving patterns, the one that yields the best decoding FER upper bound will finally be chosen for the BICM scheme. We will again demonstrate this design in the following Section V.

V. Simulation Results

This section presents our simulation results of the proposed U-UV coded BICM schemes. The theoretical decoding performance bounds and their approximations derived in Section IV are shown as benchmarks. For the simulated U-UV codes, their component codes are binary primitive BCH codes designed by the rate allocation approach of Section III. In particular, the GA based subchannel capacity estimation, i.e., **Algorithm 1**, is first utilized. The finite length rate calculation is then performed to determine the component code rates. Finally, the equal error probability rule is utilized to tune the rates to ensure the decoding performance of the BICM scheme. Within the interleaver Π, all sub-interleavers $\Pi_0, \Pi_1, \ldots, \Pi_{m-1}$ are pseudo-random interleavers with a length of $\overline{\gamma}/m$. Since this

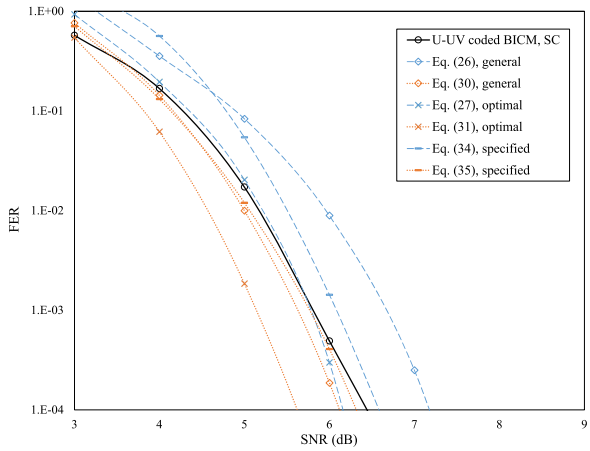

Fig. 7. SC decoding performance of the (252, 139) U-UV coded BICM with 16-QAM over the AWGN channel.

is a non-iterative decoding, Gray labelling is adopted for all modulation schemes. Both the SC and SCL decoding of U-UV codes are simulated, in which the component codes are decoded by the OSD with a decoding order determined by (9). The SNR is expressed in E_{b}/N_0, where N_0 is the noise power spectral density.

Under these settings, three 2 levels U-UV codes have been designed and simulated with 16-QAM such that there are four modulation channels, i.e., $m = 4$. They are the 2 levels (252, 139) U-UV code with component codes of length 63 and dimensions $\{k_0, k_1, k_2, k_3\} = \{7, 36, 39, 57\}$. It achieves a transmission rate of 2.2 information bits per symbol. The others are the 2 levels (252, 73) U-UV code with component codes of length 63 and dimensions $\{k_0, k_1, k_2, k_3\} = \{0, 10, 18, 45\}$, and the 2 levels (252, 183) U-UV code with component codes of length 63 and dimensions $\{k_0, k_1, k_2, k_3\} = \{24, 51, 51, 57\}$. They achieve the transmission rates of 1.16 and 2.9 information bits per symbol, respectively. Note that a code of dimension zero indicates its coded bits are all set to a predetermined symbol, e.g., 0, such that they do not carry information. The interleaving patterns for the (252, 139), (252, 73) and (252, 183) U-UV coded BICM schemes are $\mathcal{M} : \{0, 1, 2, 3\} \mapsto \{0, 1, 2, 3\}$, $\mathcal{M} : \{0, 1, 2, 3\} \mapsto \{0, 2, 1, 3\}$ and $\mathcal{M} : \{0, 1, 2, 3\} \mapsto \{0, 1, 2, 3\}$, respectively.

Figs. 7 and 8 show the SC decoding performance of the (252, 139) U-UV coded BICM scheme and the (252, 73) U-UV coded BICM scheme over the AWGN channel, respectively. The approximated theoretical SC decoding performance upper and lower bounds are shown as benchmarks. They include eqs. (26) and (30) for general U-UV coded BICM schemes and their optimal solutions as eqs. (27) and (31), and eqs. (34) and (35) for U-UV coded BICM scheme with BCH component codes. It can be seen that among all approximated performance bounds, eqs. (34) and (35) are the tightest references, since they are computed based on the component codes' weight spectrum. Meanwhile, the approximated upper and lower bounds of (27) and (31) reveal the performance potential of the U-UV coded BICM scheme. They can be approached by choosing better component codes and their subsequent rate allocation. Note that Fig. 8 shows for the (252, 73) U-UV coded BICM scheme, the specified upper bound

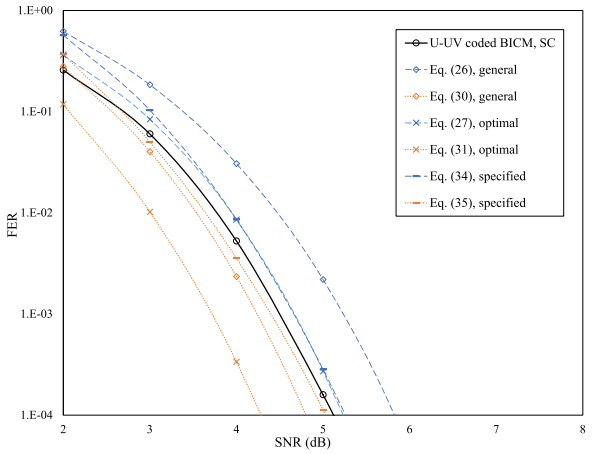

Fig. 8. SC decoding performance of the (252, 73) U-UV coded BICM with 16-QAM over the AWGN channel.

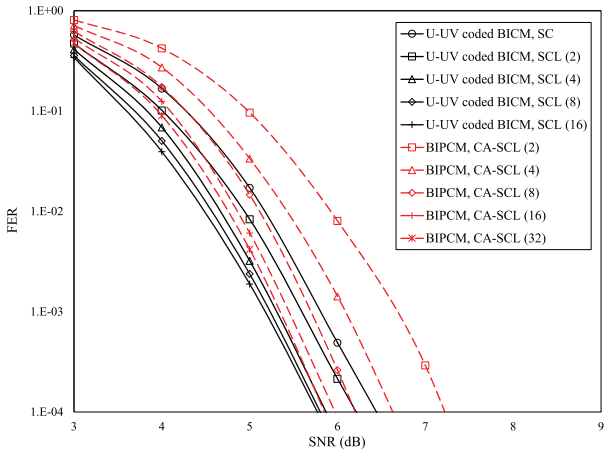

Fig. 9. SC and SCL decoding performances of the (252, 139) U-UV coded BICM with 16-QAM over the AWGN channel.

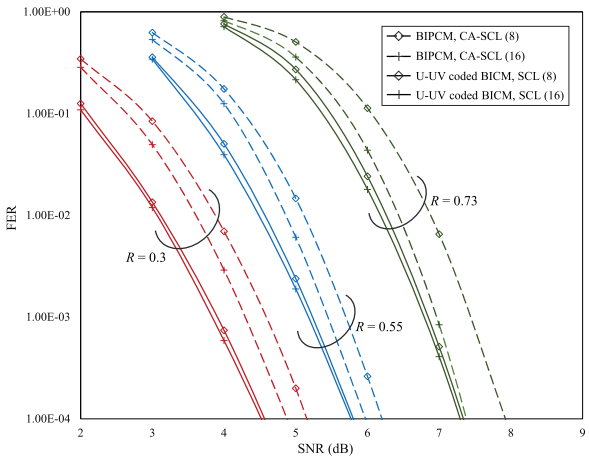

Fig. 10. FER decoding performances of the U-UV coded BICM and BIPCM with 16-QAM over the AWGN channel.

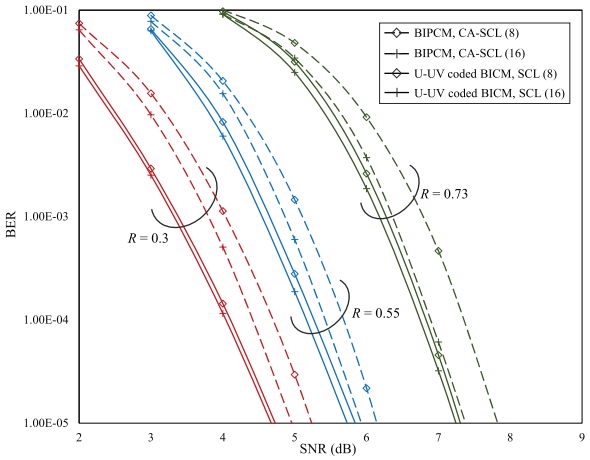

Fig. 11. BER decoding performances of the U-UV coded BICM and BIPCM with 16-QAM over the AWGN channel.

of (34) overlaps the approximated upper bound of (27). This indicates that the proposed component rate allocation method already provided an optimal solution.

Fig. 9 shows the SCL decoding performance of the (252, 139) U-UV coded BICM scheme over the AWGN channel. The SCL decoding is parameterized by its output list size l. Note that for the U-UV codes, it is ensured that the OSD of each BCH component code yields a decoding output list size that is greater than l. It can be seen that the decoding performance improves as the list size increases. They are compared with the (256, 140) BIPCM scheme [22]. The polar code is constructed using Monte Carlo simulation with a design SNR of 3dB. Note that a length-8 CRC code is outer concatenated with the polar code for enhancing its SCL decoding performance [9]. It can be seen that with the same decoding output list size, the U-UV coded BICM scheme can outperform the BIPCM scheme. However, the U-UV coded BICM scheme's performance gain decreases as the decoding output list size increases. It implies that the SCL decoding with a small output list size is more effective for the U-UV coded BICM. Note that this observation is consistent with our earlier research that considers only binary modulation [11], [43]. U-UV code's performance advantage is primarily due to the fact that in the short-to-medium length regime, channel polarization remains incomplete, limiting the performance of CRC-polar codes. The U-UV code overcomes this by transmitting component codewords through the sub-channels, so that it does not depend on complete channel polarization. With a strong component code decoding such as the OSD, its SCL decoding performance is superior to that of a CRC-polar code.

Figs. 10 and 11 further compare the U-UV coded BICM scheme with the BIPCM over a wider range of rate region, showing both of their decoding FER and bit error rate (BER) performances. The above mentioned (252, 73), (252, 139) and (252, 183) U-UV coded BICM schemes are compared with the BIPCM schemes using (256, 74), (256, 140) and (256, 186) CRC-polar codes, respectively. Thet yield the rates of 0.3, 0.55 and 0.73. The polar codes are designed using the Monte Carlo method at the SNR of 1dB, 3dB and 1dB, respectively. Again, length-8 CRC codes is used. They again show the U-UV coded BICM schemes can outperform BIPCM schemes. In particular, the performance advantage of the U-UV coded BICM enlarges in the low rate region. Table I further compares their decoding complexity, in which the average number of the floating point operations (FLOPs) and binary operations (BOPs) are measured. It can be seen that the performance advantage of the U-UV coded BICM schemes come at the

TABLE I
DECODING COMPLEXITY OF DIFFERENT BICM SCHEMES

Rate	Scheme	FLOPs	BOPs
0.3	BIPCM, CA-SCL (8)	1.46×10^4	3.06×10^4
	BIPCM, CA-SCL (16)	2.84×10^4	5.67×10^4
	proposed, SCL (8)	4.37×10^5	1.75×10^6
	proposed, SCL (16)	9.24×10^5	3.27×10^6
0.55	BIPCM, CA-SCL (8)	1.94×10^4	3.82×10^4
	BIPCM, CA-SCL (16)	4.02×10^4	7.26×10^4
	proposed, SCL (8)	2.83×10^5	1.27×10^6
	proposed, SCL (16)	7.50×10^5	2.52×10^6
0.73	BIPCM, CA-SCL (8)	2.22×10^4	4.42×10^4
	BIPCM, CA-SCL (16)	4.66×10^4	8.54×10^4
	proposed, SCL (8)	1.02×10^5	4.75×10^5
	proposed, SCL (16)	1.68×10^5	6.55×10^5

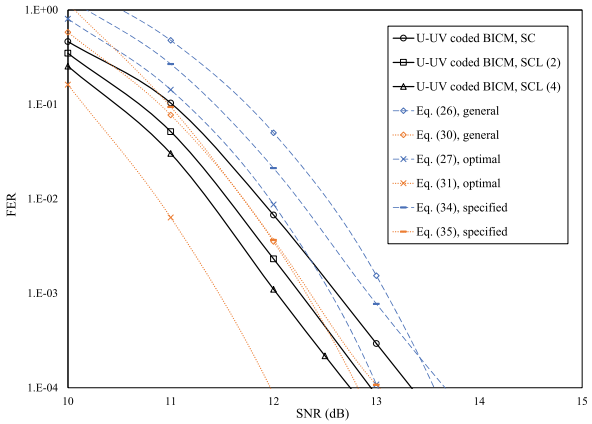

Fig. 12. SC and SCL decoding performances of the (504, 304) U-UV coded BICM with 256-QAM over the AWGN channel.

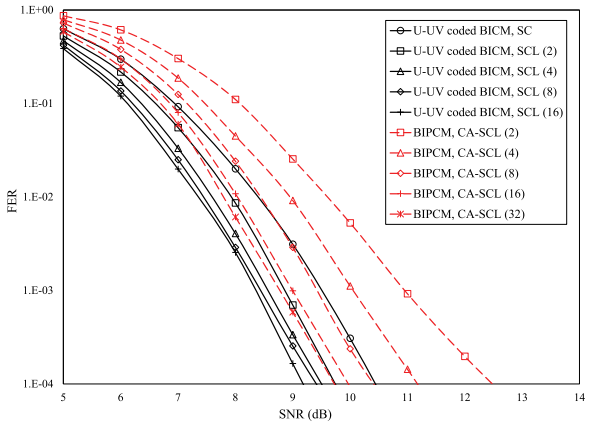

Fig. 13. SC and SCL decoding performances of the (252, 139) U-UV coded BICM with 16-QAM over the Rayleigh fading channel.

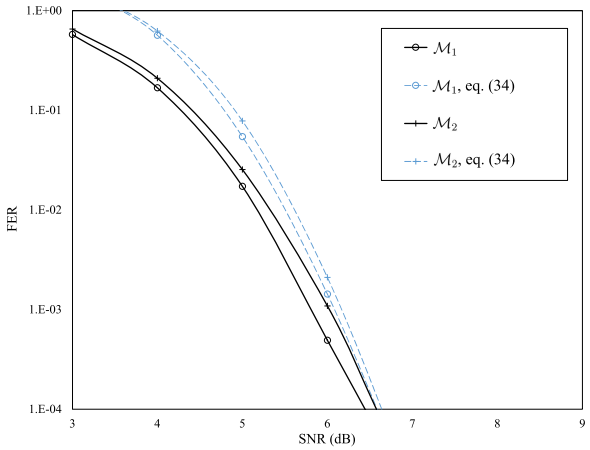

Fig. 14. SC decoding performance of the (252, 139) U-UV coded BICM with 16-QAM and different interleavers over the AWGN channel.

cost of a higher decoding complexity. This is mainly due to the OSD in decoding the component codes, whose complexity is exponential in the decoding order [43]. In this work, the OSD orders are chosen according to (9) to generate the ML decoding performance of component codes. This also explains why SCL decoding complexity of the U-UV coded BICM scheme decreases for a higher rate code, which is opposite to the BIPCM scheme. However, it should be pointed out that the OSD complexity can be effectively reduced by various approaches, such as the box-and-match algorithm [44] or the early termination that terminates the decoding once an ML codeword is identified. Moreover, it is possible that smaller OSD orders can also enable the U-UV coded BICM scheme to yield a similar decoding performance. However, investigating low-complexity decoding of the BICM scheme is beyond the scope of this work, which will be considered in future.

Fig. 12 shows the SC and SCL decoding FER performances of the 3 levels (504, 304) U-UV coded BICM with the Gray labelling 256-QAM over the AWGN channel. It achieves a transmission rate of 4.83 information bits per symbol. In this case, there are eight component codes and eight modulation channels, i.e., $\gamma = m = 8$. The component codes are of length 63 and dimensions $\{k_0, k_1, k_2, k_3, k_4, k_5, k_6, k_7\} = \{0, 16, 24, 51, 36, 57, 57, 63\}$. The interleaving pattern is $\mathcal{M} : \{0, 1, 2, 3, 4, 5, 6, 7\} \mapsto \{0, 2, 1, 4, 3, 6, 5, 7\}$. Similarly, Fig. 12 again shows the SC decoding performance of this U-UV coded BICM scheme is enveloped by the specified ML decoding upper and the approximated lower bounds of (34) and (35), respectively.

Fig. 13 shows the SC and SCL decoding performances of the (252, 139) U-UV coded BICM with the Gray labelling 16-QAM over the Rayleigh fading channel. It is a fast fading channel with fading coefficients changing independently over symbols. It is assumed that the channel state information is known by the receiver so that coherent detection can be realized. As comparison, SCL decoding performance of the (256, 140) BIPCM scheme is also provided. The polar code is designed by the Monte Carlo method at the SNR of 9 dB and it is concatenated with a length-8 CRC. Again, it shows the U-UV coded BICM scheme can significantly outperform the BIPCM scheme, yielding the greater coding gains than the case in the AWGN channel.

Finally, Fig. 14 demonstrates the impact of different interleaver designs by comparing the SC decoding performances of the above mentioned 2 levels (252, 139) U-UV coded BICM scheme. The two interleaving patterns are $\mathcal{M}_1 : \{0, 1, 2, 3\} \mapsto \{0, 1, 2, 3\}$ and $\mathcal{M}_2 : \{0, 1, 2, 3\} \mapsto \{0, 2, 1, 3\}$. Note that with the Gray labeling 16-QAM and four component codes, there are only two subchannel capacity polarizations, which can be yielded by these two interleaving patterns, respectively. The decoding FER upper

bound, i.e., eq. (34), of the two U-UV coded BICM schemes are also provided. It can be seen that interleaving pattern $\mathcal{M}_1$ prevails $\mathcal{M}_2$. The theoretical upper bound also shows the same conclusion. This echoes our discussions in Section IV-B that the theoretical decoding performance bounds can enable us to design the interleaving pattern without incurring the exhaustive simulations.

VI. Conclusion

This paper has proposed the design of BICM scheme for the U-UV codes, in order to realize spectrally efficient transmission for this competent short-to-medium length channel code. The interleaver has been designed such that the component code rates can be allocated based on the estimated polarized subchannel capacities. Two modulation subchannel capacity estimation methods have been introduced. They are based on the Bhattacharyya parameter and the GA, respectively. With the estimated subchannel capacities, the finite length rate and the equal error probability rule can be further applied to design the component code rates. The theoretical SC decoding performance bounds and their approximations of the U-UV coded BICM scheme have been analyzed. These performance characterizations not only provide theoretical benchmarks for our simulations, but also helps the design of the BICM scheme. Using BCH codes as the component codes, extensive simulation study has been conducted on the proposed BICM scheme. It has shown that with the proposed design, the U-UV coded BICM can provide competent performance with both the SC and the SCL decoding, verifying the theoretical performance analysis. Meanwhile, our results have also shown that the U-UV coded BICM scheme can outperform the existing BIPCM scheme.

References

[1] A. Hocquenghem, "Codes correcteurs erreurs," *Chiffres*, vol. 2, pp. 147–156, Sep. 1959.

[2] R. C. Bose and D. K. Ray-Chaudhuri, "On a class of error correcting binary group codes," *Inf. Control*, vol. 3, no. 1, pp. 68–79, Mar. 1960.

[3] H. Ma and J. Wolf, "On tail biting convolutional codes," *IEEE Trans. Commun.*, vol. COM-34, no. 2, pp. 104–111, Feb. 1986.

[4] E. Arikan, "Channel polarization: A method for constructing capacity-achieving codes for symmetric binary-input memoryless channels," *IEEE Trans. Inf. Theory*, vol. 55, no. 7, pp. 3051–3073, Jul. 2009.

[5] I. Tal and A. Vardy, "List decoding of polar codes," *IEEE Trans. Inf. Theory*, vol. 61, no. 5, pp. 2213–2226, May 2015.

[6] K. Niu and K. Chen, "CRC-aided decoding of polar codes," *IEEE Commun. Lett.*, vol. 16, no. 10, pp. 1668–1671, Oct. 2012.

[7] E. Arıkan, "From sequential decoding to channel polarization and back again," 2019, *arXiv:1908.09594*.

[8] M. P. C. Fossorier and S. Lin, "Soft-decision decoding of linear block codes based on ordered statistics," *IEEE Trans. Inf. Theory*, vol. 41, no. 5, pp. 1379–1396, Sep. 1995.

[9] Q. Zhang, A. Liu, X. Pan, and K. Pan, "CRC code design for list decoding of polar codes," *IEEE Commun. Lett.*, vol. 21, no. 6, pp. 1229–1232, Jun. 2017.

[10] J. Piao, K. Niu, J. Dai, and C. Dong, "Approaching the normal approximation of the finite blocklength capacity within 0.025 dB by short polar codes," *IEEE Wireless Commun. Lett.*, vol. 9, no. 7, pp. 1089–1092, Jul. 2020.

[11] J. Cheng and L. Chen, "BCH based U-UV codes and its decoding," in *Proc. IEEE Int. Symp. Inf. Theory (ISIT)*, Jul. 2021, pp. 1433–1438.

[12] I. Uez-Corbella and J.-P. Tillich, "Attaining capacity with iterated (UlU+V) codes based on AG codes and Koetter–Vardy soft decoding," in *Proc. IEEE Int. Symp. Inf. Theory (ISIT)*, Aachen, Germany, Jun. 2017, pp. 6–10.

[13] M. Plotkin, "Binary codes with specified minimum distance," *IRE Trans. Inf. Theory*, vol. 6, no. 4, pp. 445–450, Sep. 1960.

[14] P. Trifonov and P. Semenov, "Generalized concatenated codes based on polar codes," in *Proc. 8th Int. Symp. Wireless Commun. Syst.*, Aachen, Germany, Nov. 2011, pp. 442–446.

[15] H. Imai and S. Hirakawa, "A new multilevel coding method using error-correcting codes," *IEEE Trans. Inf. Theory*, vol. IT-23, no. 3, pp. 371–377, May 1977.

[16] G. Ungerboeck, "Channel coding with multilevel/phase signals," *IEEE Trans. Inf. Theory*, vol. IT-28, no. 1, pp. 55–67, Jan. 1982.

[17] E. Zehavi, "8-PSK trellis codes for a Rayleigh channel," *IEEE Trans. Commun.*, vol. 40, no. 5, pp. 873–884, May 1992.

[18] G. Caire, G. Taricco, and E. Biglieri, "Bit-interleaved coded modulation," *IEEE Trans. Inf. Theory*, vol. 44, no. 3, pp. 927–946, May 1998.

[19] X. Li and J. A. Ritcey, "Bit-interleaved coded modulation with iterative decoding," *IEEE Commun. Lett.*, vol. 1, no. 6, pp. 169–171, Nov. 1997.

[20] M. Seidl, A. Schenk, C. Stierstorfer, and J. B. Huber, "Polar-coded modulation," *IEEE Trans. Commun.*, vol. 61, no. 10, pp. 4108–4119, Oct. 2013.

[21] K. Chen, K. Niu, and J.-R. Lin, "An efficient design of bit-interleaved polar coded modulation," in *Proc. IEEE 24th Int. Symp. Pers. Indoor Mobile Radio Commun. (PIMRC)*, London, U.K., Sep. 2013, pp. 693–697.

[22] H. Mahdavifar, M. El-Khamy, J. Lee, and I. Kang, "Polar coding for bit-interleaved coded modulation," *IEEE Trans. Veh. Technol.*, vol. 65, no. 5, pp. 3115–3127, May 2016.

[23] V. Bioglio, C. Condo, and I. Land, "Design of polar codes in 5G new radio," *IEEE Commun. Surveys Tuts.*, vol. 23, no. 1, pp. 29–40, 1st Quart., 2021.

[24] P. Chen, M. Xu, B. Bai, and X. Ma, "Design of polar coded 64-QAM," in *Proc. 9th Int. Symp. Turbo Codes Iterative Inf. Process. (ISTC)*, Brest, France, Sep. 2016, pp. 251–255.

[25] X. Wu, M. Qiu, and J. Yuan, "Partially information coupled bit-interleaved polar coded modulation," *IEEE Trans. Commun.*, vol. 69, no. 10, pp. 6409–6423, Oct. 2021.

[26] M. Chiu, "Analysis and design of polar-coded modulation," *IEEE Trans. Commun.*, vol. 70, no. 3, pp. 1508–1521, Mar. 2022.

[27] M. Chiu, "Nonbinary I-polar coded modulation," *IEEE Trans. Inf. Theory*, vol. 68, no. 4, pp. 2266–2280, Apr. 2022.

[28] O. Iscan, R. Böhnke, and W. Xu, "Shaped polar codes for higher order modulation," *IEEE Commun. Lett.*, vol. 22, no. 2, pp. 252–255, Feb. 2018.

[29] U. U. Fayyaz, "Symbol mapping design for bit-interleaved polar-coded modulation with iterative decoding," *IEEE Commun. Lett.*, vol. 23, no. 1, pp. 32–35, Jan. 2019.

[30] M. Seidl, A. Schenk, C. Stierstorfer, and J. B. Huber, "Multilevel polar-coded modulation," in *Proc. IEEE Int. Symp. Inf. Theory*, Jul. 2013, pp. 1302–1306.

[31] K. Chen, K. Niu, and J. Lin, "Polar coded modulation with optimal constellation labeling," in *Proc. Nat. Doctoral Academic Forum Inf. Commun. Technol.*, Beijing, China, Aug. 2013, pp. 1–5.

[32] P. R. Balogun, I. D. Marsland, R. H. Gohary, and H. Yanikomeroglu, "Polar code design for irregular multidimensional constellations," *IEEE Access*, vol. 5, pp. 21941–21953, 2017.

[33] G. Bocherer, T. Prinz, P. Yuan, and F. Steiner, "Efficient polar code construction for higher-order modulation," in *Proc. IEEE Wireless Commun. Netw. Conf. Workshops (WCNCW)*, San Francisco, CA, USA, Mar. 2017, pp. 1–6.

[34] P. Chen and B. Bai, "Design and performance of the polar coded modulation for high mobility communications," in *Proc. IEEE 87th Veh. Technol. Conf. (VTC Spring)*, Porto, Portugal, Jun. 2018, pp. 1–5.

[35] H. Khoshnevis, I. Marsland, and H. Yanikomeroglu, "Throughput-based design for polar-coded modulation," *IEEE Trans. Commun.*, vol. 67, no. 3, pp. 1770–1782, Mar. 2019.

[36] P. Trifonov, "Design of multilevel polar codes with shaping," in *Proc. IEEE Int. Symp. Inf. Theory (ISIT)*, Espoo, Finland, Jun. 2022, pp. 2160–2165.

[37] H. Yao, J. Du, and A. Vardy, "Polar coded modulation via hybrid bit labeling," in *Proc. IEEE Int. Symp. Inf. Theory (ISIT)*, Espoo, Finland, Jun. 2022, pp. 980–985.

[38] P. Trifonov, "Efficient design and decoding of polar codes," *IEEE Trans. Commun.*, vol. 60, no. 11, pp. 3221–3227, Nov. 2012.

[39] H. Mahdavifar, M. El-Khamy, J. Lee, and I. Kang, "Performance limits and practical decoding of interleaved reed-solomon polar concatenated codes," *IEEE Trans. Commun.*, vol. 62, no. 5, pp. 1406–1417, May 2014.

[40] P. Trifonov and V. Miloslavskaya, "Polar subcodes," *IEEE J. Sel. Areas Commun.*, vol. 34, no. 2, pp. 254–266, Feb. 2016.
[41] H. Saber and I. Marsland, "Design of generalized concatenated codes based on polar codes with very short outer codes," *IEEE Trans. Veh. Technol.*, vol. 66, no. 4, pp. 3103–3115, Apr. 2017.
[42] D. N. Bailon, M. Bossert, J. Thiers, and J. Freudenberger, "Concatenated codes based on the Plotkin construction and their soft-input decoding," *IEEE Trans. Commun.*, vol. 70, no. 5, pp. 2939–2950, May 2022.
[43] W. Chen, J. Cheng, C. Wu, and L. Chen, "BCH based U-UV codes and its SCL decoding," unpublished.
[44] A. Valembois and M. Fossorier, "Box and match techniques applied to soft-decision decoding," *IEEE Trans. Inf. Theory*, vol. 50, no. 5, pp. 796–810, May 2004.
[45] J. G. Proakis and M. Salehi, *Digital Communications*. New York, NY, USA: McGraw-Hill, 2008.
[46] Y. Polyanskiy, H. Vincent Poor, and S. Verdu, "Channel coding rate in the finite blocklength regime," *IEEE Trans. Inf. Theory*, vol. 56, no. 5, pp. 2307–2359, May 2010.
[47] D. Goldin and D. Burshtein, "Performance bounds of concatenated polar coding schemes," *IEEE Trans. Inf. Theory*, vol. 65, no. 11, pp. 7131–7148, Nov. 2019.
[48] C. E. Shannon, "Probability of error for optimal codes in a Gaussian channel," *Bell Syst. Tech. J.*, vol. 38, no. 3, pp. 611–656, May 1959.
[49] G. Poltyrev, "Bounds on the decoding error probability of binary linear codes via their spectra," *IEEE Trans. Inf. Theory*, vol. 40, no. 4, pp. 1284–1292, Jul. 1994.
[50] M. Terada, J. Asatani, and T. Koumoto. *Weight Distribution*. Accessed: May 17, 2022. [Online]. Available: http://www.isec.ec.okayama-u.ac.jp/home/kusaka/wd

Changyu Wu received the B.Sc. degree in electronic information science and technology and the M.Sc. degree in communication and information systems from Sun Yat-sen University, Guangzhou, China, in 2019 and 2022, respectively. His research interests include channel coding and data communications.

Wenhao Chen received the B.Sc. degree in information engineering from Sun Yat-sen University, Guangzhou, China, in 2021, where he is currently pursuing the M.Sc. degree in information and communication engineering. His research interests include channel coding and data communications.

Li Chen (Senior Member, IEEE) received the B.Sc. degree in applied physics from Jinan University, Guangzhou, China, in 2003, and the M.Sc. degree in communications and signal processing and the Ph.D. degree in communications engineering from Newcastle University, U.K., in 2004 and 2008, respectively. From 2007 to 2010, he was a Research Associate with Newcastle University. In 2010, he returned to China as a Lecturer with the School of Information Science and Technology, Sun Yat-sen University, Guangzhou. From 2011 to 2012, he was a Visiting Researcher with the Institute of Network Coding, The Chinese University of Hong Kong, where he was an Associate Professor and a Professor from 2011 and 2016. Since 2013, he has been the Associate Head with the Department of Electronic and Communication Engineering (ECE). From July 2015 to October 2015, he was a Visitor with the Institute of Communications Engineering, Ulm University, Germany. From October 2015 to June 2016, he was a Visiting Associate Professor with the Department of Electrical Engineering, University of Notre Dame, Notre Dame, IN, USA. From 2017 to 2020, he was the Deputy Dean with the School of Electronics and Communication Engineering. His research interests include information theory, error-correction codes, and data communications. He is a Senior Member of the Chinese Institute of Electronics (CIE). He is a member of the IEEE Information Theory Society Board of Governors and its External Nomination Committee and the Chair of its Conference Committee. He is also the Chair of the IEEE Information Theory Society Guangzhou Chapter. He has been organizing several international conferences and workshops, including the 2018 IEEE Information Theory Workshop (ITW) at Guangzhou and the 2022 IEEE East Asian School of Information Theory (EASIT) at Shenzhen, for which he is the General Co-Chair. He is also the TPC Co-Chair of 2022 IEEE/CIC International Conference on Communications in China (ICCC) at Foshan. He likes reading and photography. He is an Associate Editor of IEEE TRANSACTIONS ON COMMUNICATIONS.

Huazi Zhang (Senior Member, IEEE) received the B.Sc. and Ph.D. degrees from the Institute of Information and Communication Engineering, Zhejiang University, in 2008 and 2013, respectively. From 2011 to 2013, he was a Visiting Researcher with the Department of Electrical and Computer Engineering, North Carolina State University, Raleigh, NC, USA. From 2013 to 2014, he was a Research Fellow with the School of Computer Engineering, Nanyang Technological University, Singapore. From 2014 to 2015, he was a Research Scholar with the Department of Electrical and Computer Engineering, University of Florida, Gainesville, FL, USA. He joined Huawei Technologies Company Ltd., in 2015. Since then, he has engaged in research projects on advanced wireless communications involving channel coding and signal processing techniques, and engaged in multiple standardization activities. His contribution led to the adoption of many state-of-the-art research results into 5G standards, as well as the subsequent commercial rollout. He has over 100 journals, conference publications, and patent applications in the areas of coding techniques, wireless communications, and signal processing. His current research interests are channel coding, information theory, and signal processing for wireless communications, with a focus on theoretical analysis, algorithm design, and hardware implementations for 5G and beyond. He has been serving on the Technical Program Committee of communications theory, wireless communications, and signal processing symposia for IEEE GLOBECOM and ICC since 2013. He was an Exemplary Reviewer of IEEE TRANSACTIONS ON COMMUNICATIONS in 2014.